# Modifications of turbulence and turbulent transport associated with a bias-induced confinement transition in the Large Plasma Device

T. A. Carter[1,2,a] and J. E. Maggs[1]
[1]*Department of Physics and Astronomy, University of California, Los Angeles, California 90095-1547, USA*
[2]*Center for Multiscale Plasma Dynamics, University of California, Los Angeles, California 90095-1547, USA*

(Received 14 July 2008; accepted 9 December 2008; published online 21 January 2009)

Azimuthal flow is driven in the edge of the Large Plasma Device (LAPD) [W. Gekelman *et al.*, Rev. Sci. Instrum. **62**, 2875 (1991)] through biasing a section of the vacuum vessel relative to the plasma source cathode. As the applied bias exceeds a threshold, a transition in radial particle confinement is observed, evidenced by a dramatic steepening in the density profile, similar to the L- to H-mode transition in toroidal confinement devices. The threshold behavior and dynamic behavior of radial transport is related to flow penetration and the degree of spatial overlap between the flow shear and density gradient profiles. An investigation of the changes in turbulence and turbulent particle transport associated with the confinement transition is presented. Two-dimensional cross-correlation measurements show that the spatial coherence of edge turbulence in LAPD changes significantly with biasing. The azimuthal correlation in the turbulence increases dramatically, while the radial correlation length is little altered. Turbulent amplitude is reduced at the transition, particularly in electric field fluctuations, but the dominant change observed is in the cross-phase between density and electric field fluctuations. The changes in cross-phase lead to a suppression and then apparent reversal of turbulent particle flux as the threshold is exceeded. © *2009 American Institute of Physics*. [DOI: 10.1063/1.3059410]

## I. INTRODUCTION

Turbulence has long been recognized as the dominant cause of cross-field transport in magnetically confined plasmas.[1] Significant progress in the effort to confine plasmas for fusion energy came with the discovery of the high-confinement mode or H-mode, where the spontaneous formation of an edge transport barrier occurs after the heating power exceeds a threshold.[2] A key characteristic of these transport barriers is the presence of a localized, nonuniform radial electric field with associated cross-field $E\times B$ flow and flow shear.[3,4] The important role of radial electric field in the confinement transition was first demonstrated clearly in experiments in the Continuous Current Tokamak,[5,6] where biasing was used to establish a radial electric field and trigger an H-mode confinement transition. Since these pioneering experiments, biasing has been used on a number of confinement devices to study transport barrier formation and turbulence modification.[7–13]

Flow and flow shear can modify turbulence and transport through a number of processes. First, the shear can lead to radial decorrelation or "shearing apart" of turbulent eddies, reducing their radial extent and therefore their transport effectiveness.[14] Furthermore, the amplitude of turbulent fluctuations can be reduced through the modification of the nonlinearly saturated level of the turbulence.[3] Finally, electrostatically driven particle transport is dependent on the correlation between density and electric field fluctuations in low frequency turbulence (where $E\times B$ is the dominant particle response):

$$\Gamma_n = \langle n v_r \rangle = \frac{\langle n E_\theta \rangle}{B} = \frac{2}{B}\int_0^\infty |n(\omega)||E_\theta(\omega)|\gamma_{n,E_\theta}(\omega)\cos[\theta_{n,E_\theta}(\omega)]d\omega, \quad (1)$$

where $n(\omega)$ and $E_\theta(\omega)$ are the Fourier transforms of density and azimuthal electric field, respectively, $\gamma_{n,E_\theta}$ is the cross-coherency between $n$ and $E_\theta$, and $\theta_{n,E_\theta}$ is the cross-phase between density and electric field fluctuations.[15] Flow and flow shear can modify both the cross-phase and cross-coherency between density and potential fluctuations, leading to a reduction of transport even in the absence of amplitude reduction.[16,17]

Changes in turbulence and transport associated with azimuthal flow have been investigated in the Large Plasma Device (LAPD) at UCLA. Flows are driven through biasing the vacuum chamber wall relative to the plasma source.[18–20] Excitation of the Kelvin–Helmholtz instability has been observed in LAPD when a strong flow gradient is imposed (through modification of the magnetic topology).[19,20] For flow driven in a straight-magnetic-field-line configuration in LAPD (resulting in smaller but non-negligible flow shear), a transition in particle confinement is observed. Models of diffusive particle transport and changes in transport are presented in an earlier publication,[18] where it is reported that transport rates change from Bohm to classical due to edge rotation. The observation of a confinement transition in a simple magnetic geometry provides the opportunity to

[a]Electronic mail: tcarter@physics.ucla.edu.

 

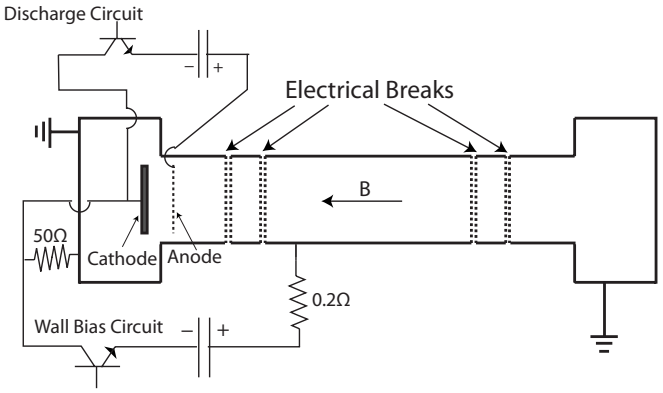


FIG. 1. Schematic of LAPD including wall biasing circuit.

perform a detailed study of modifications of turbulence and turbulent transport in a system free from complications associated with toroidal systems (e.g., field line curvature, poloidal asymmetry, trapped particles). Good diagnostic access to LAPD provides for detailed measurements of the spatial and temporal characteristics of the turbulence.

Here we summarize the primary results reported in this paper. Measured turbulent transport flux is reduced and then suppressed, leading to a confinement transition, as the applied bias is increased. The threshold in the applied bias is linked to radial penetration of the driven azimuthal flow. Two-dimensional measurements of the turbulent correlation function show that the azimuthal correlation increases dramatically during biasing, with the high-$m$-number modes involved in turbulent transport becoming spatially coherent. However, no significant change in the radial correlation length is observed associated with the confinement transition. As the bias is increased above threshold, there is an apparent reversal in the particle flux (indicating inward transport). The peak amplitude of density and electric field fluctuations do decrease, but the reduction is only slight and does not fully explain the transport flux reduction. The cross-phase between density and electric field fluctuations changes significantly as the threshold for confinement transition is reached, and explains the reduction and reversal of the measured transport flux. The dynamics of the transition have also been studied and show a correlation between transport suppression and the overlap of the flow (shear) profile and the density (gradient) profile.

## II. EXPERIMENTAL SETUP

The experiments were performed in the upgraded Large Plasma Device (LAPD),[21] which is part of the Basic Plasma Science Facility (BaPSF) at UCLA. The vacuum chamber of LAPD is 18 m long and 1 m in diameter and is surrounded by solenoidal magnetic field coils. The plasma is generated by a cathode discharge.[22] The cathode is 73 cm in diameter and is located at one end of the vacuum chamber, as shown schematically in Fig. 1. A molybdenum mesh anode is situated 50 cm away from the cathode. A bias of 40–60 V is applied between the cathode and anode using a solid-state switch,[23] resulting in 3–6 kA of discharge current. An important aspect of the operation of the plasma source is the generation of primary electrons with energy comparable to the anode-cathode bias voltage. The mesh anode is 50% transparent, allowing half of these primaries to travel down the magnetic field into the main chamber leading to ionization and heating of the bulk plasma. The cathode is situated at the mouth of the solenoid and therefore sits in a region of flaring magnetic field. The flared magnetic field maps the 73 cm diameter cathode to a ~56 cm diameter region in the main chamber. Primary electrons from the source are isolated to this region in the chamber and lead to a fast electron tail for $r \lesssim 28$ cm. Typical plasma parameters in LAPD discharges are $n_e \lesssim 5 \times 10^{12}$ cm$^{-3}$, $T_e \sim 7$ eV, $T_i \sim 1$ eV, and $B < 2$ kG. In the experiments reported here, the primary plasma species was singly ionized helium and the magnetic field strength used was 400 G. Modeling[18] and spectroscopic measurements show that the ionization fraction of the LAPD plasma is $\gtrsim 50\%$ and therefore Coulomb collisions are the most important collisional process. However, neutral collisions (charge exchange in particular) are important for establishing the radial current during biasing.

Measurements of density, temperature, floating potential, and their fluctuations are made using Langmuir probes. A four-tip probe with 0.76 mm diameter tantalum tips arranged in a diamond pattern is used as a triple Langmuir probe and particle flux probe. Two tips are separated 3 mm along the field and are used as a double probe to measure ion saturation current ($I_{\mathrm{sat}} \propto n_e \sqrt{T_e}$). The remaining two tips are separated 3 mm perpendicular to the field and measure floating potential for deriving azimuthal electric field fluctuations and temperature using the triple Langmuir probe method.[24] Radial particle transport can be evaluated directly using measured density and electric field fluctuations through Eq. (1). Flows are measured using a Gundestrup (Mach) probe with six faces.[25] The flow measurements are corrected for the finite acceptance angle of the probe faces, which are smaller than the ion gyroradius.[26]

Using the difference in floating potential to determine the azimuthal electric field is problematic in the presence of fast electron tails, such as exist on field lines connected to the cathode source. In the presence of fast electrons, differences in floating potential may no longer be proportional to differences in plasma potential and thus may not accurately measure the electric field. In addition, the fast electron tail, which sets floating potential, is much less collisional than the bulk plasma so that the floating potential is no longer a localized quantity. This delocalization skews the correlation with locally measured density fluctuations and thereby affects the flux measurement. Measurements of $I_{\mathrm{sat}}$ are made with a double-Langmuir probe biased to 70 V to reject primary electrons, and therefore should not be affected by the fast electron tail. Thus, in this study, we report on the properties of ion saturation fluctuations everywhere in the plasma column. Properties of electric field fluctuations and cross-correlation flux measurements are presented everywhere in the plasma column, but a caution is issued in regard to measurements made on field lines where primary electrons are present ($r \lesssim 28$ cm).

The edge plasma in LAPD is rotated through biasing the vacuum vessel wall positively with respect to the source

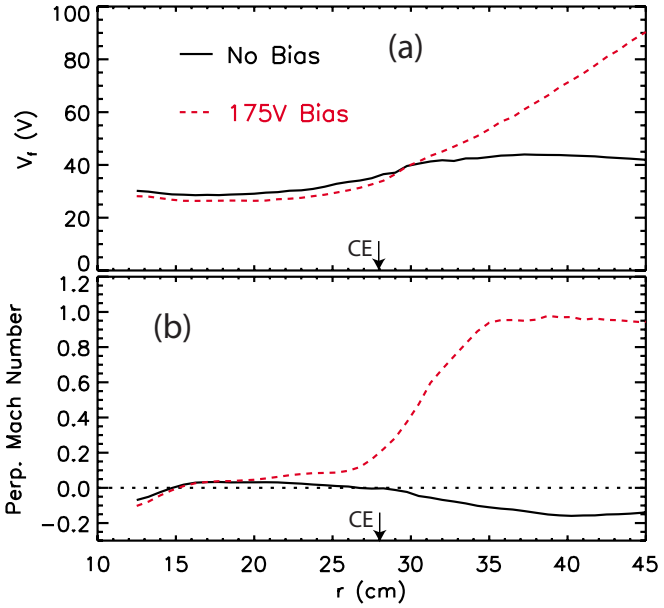


FIG. 2. (Color online) Radial profiles of (a) floating potential and (b) perpendicular Mach number for no bias and 175 V bias. Note the radial location of field lines that connect to the cathode edge are marked with "CE" in this figure and subsequent figures.

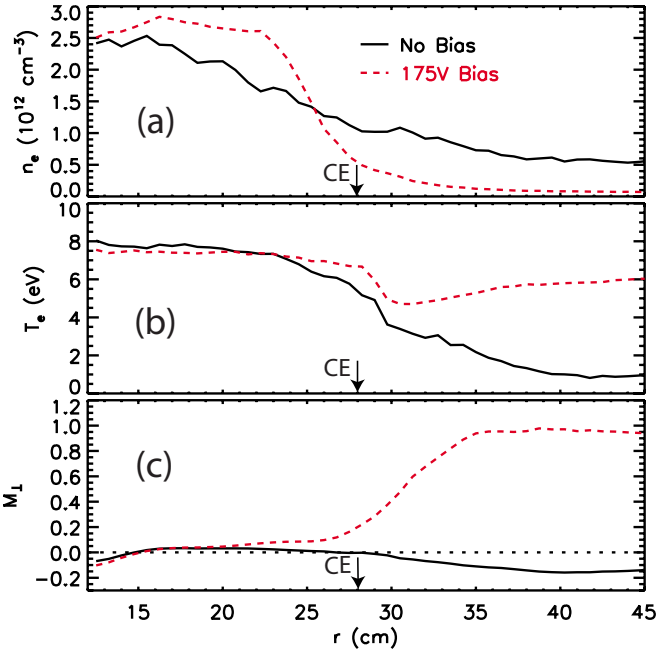


FIG. 3. (Color online) Profiles of (a) density, (b) electron temperature, and (c) Mach number before and after a confinement transition.

cathode. Figure 1 shows a schematic of the LAPD along with the rotation bias circuit, which includes a capacitor bank and an insulated gate bipolar transistor switch. The rotation bias is pulsed, with the switch closed for 4 ms during the steady portion (current flat-top) of the LAPD discharge. Typical bias voltages are on the order of 100 V, and result in around 100 A of peak radial current. The radial current provides the torque (through $J\times B$ forces) needed to spin up the plasma. The measured current is consistent with ions carrying the radial current through ion-neutral collisions (Pederson conductivity).[18] The ions carry the current radially until they reach field lines which connect to the cathode in the plasma source, where the current closes via parallel electron currents. The influence of the applied wall bias is therefore limited to regions of the plasma that are not connected along the magnetic field to the cathode source. This is demonstrated in Fig. 2(a), which shows the measured floating potential as a function of radius for no bias and a bias of 175 V. Measurements shown in this figure (and subsequent figures) are made with a 1 cm radial resolution through moving a single probe on a shot-to-shot basis. The trace shown is the result of a time average over 1.3 ms of data during the flat-top of the LAPD discharge current pulse. Field lines in the region $r\lesssim 28$ cm connect to the cathode, and the floating potential is unchanged by the applied bias in this region. Note that in this figure (and many following figures) the radial location of the field lines which connect to the cathode edge is marked with "CE." Measurements of azimuthal flow (Mach number) for the same case are shown in Fig. 2(b), indicating that driven flows are also localized to field lines not connected to the plasma source.

## III. EXPERIMENTAL RESULTS

### A. Threshold for confinement transition

A radial particle confinement transition is observed with biasing.[18] Figure 3 shows profiles of plasma density, electron temperature, and perpendicular Mach number for two cases: unbiased and 175 V bias. Without bias, radial turbulent particle transport causes the density profile to extend well past the cathode edge, with a fairly gentle gradient ($L_n=|\nabla \ln n|^{-1}\sim 10$ cm), as shown in Fig. 3(a). For comparison, the ion sound gyroradius is $\rho_s\sim 1.2$ cm (helium, $T_e\sim 6$ eV, $B=400$ G), and the ion gyroradius is $\rho_i\sim 0.5$ cm ($T_i\sim 1$ eV). In the biased case, the measured density profile steepens dramatically ($L_n\sim 4$ cm). Detailed transport modeling of the LAPD plasma shows that the profile before biasing is consistent with radial diffusion at the Bohm rate. The steepened profile after biasing is consistent with classical collisional diffusion, a factor of $\sim$100 drop in the diffusion coefficient.[18] In the rotating plasma, the density profile is essentially set by the plasma production source profile since the radial transport rates are so slow.

The electron temperature profiles measured using the triple probe technique are shown in Fig. 3(b). The electron temperature drops rapidly past the edge of the cathode. The electron beam from the cathode acts primarily as a heat source once the plasma is formed. The fully formed plasma column is hot and dense enough that the tail of the Maxwellian distribution dominates the beam electrons in the ionization process. In the rotating plasma, the electron temperature is elevated in the region outside the plasma source, perhaps due to frictional heating from neutral drag. The Mach-probe-measured azimuthal flow profile, with and without bias, is repeated in Fig. 3(c) for reference.

The observed profile steepening occurs for bias voltages

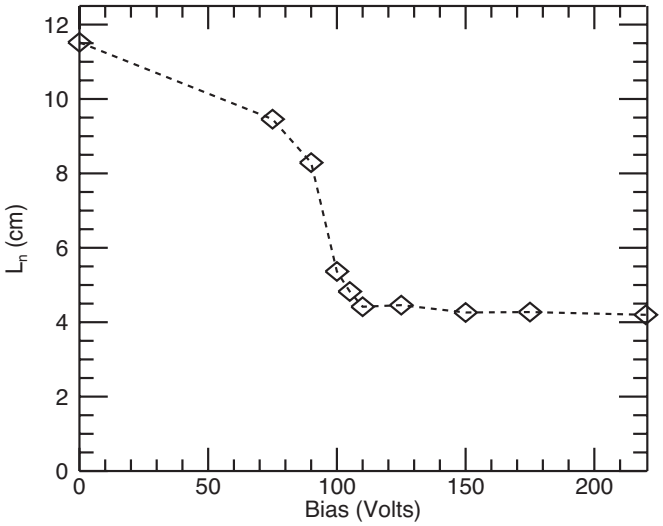


FIG. 4. Minimum radial density gradient scale length as a function of applied bias. (This figure reprinted from Ref. 18.)

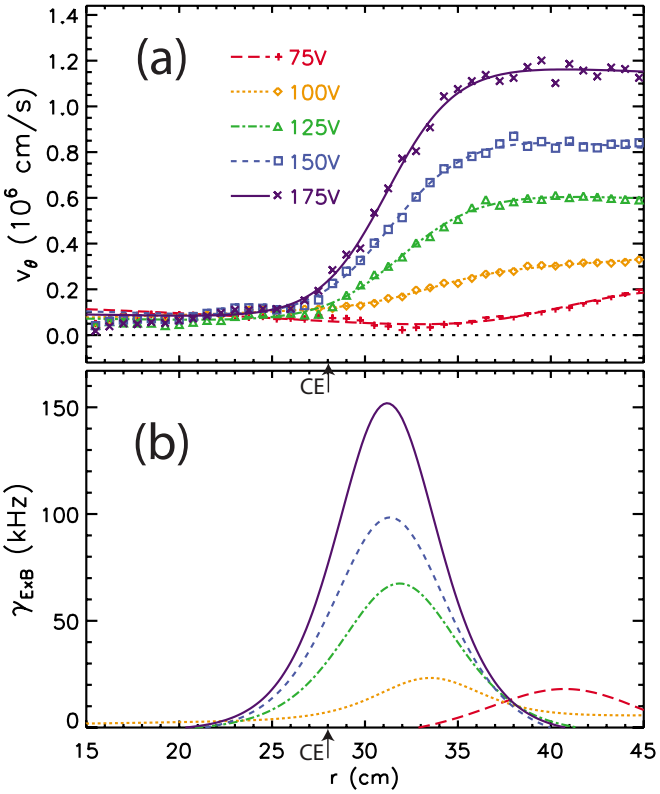


FIG. 5. (Color online) For several bias values: (a) Radial profile of azimuthal velocity, with fit. (b) Radial profile of shearing rate, derived from fit to azimuthal velocity profile.

above a threshold value. Figure 4 shows the minimum density gradient scale length ($L_n$) versus bias voltage. For biases above ~100 V, the density gradient scale length decreases dramatically, indicating a transition in the radial particle confinement. As the bias is increased, the density gradient scale length saturates (near $L_n \sim 4$ cm), consistent with modeling which shows that transport beyond the confinement transition threshold is suppressed to the irreducible lowest level set by classical transport.[18]

The threshold for confinement transition in LAPD appears to be set by radial penetration of the bias-driven flow. Figure 5(a) shows the radial profile of azimuthal flow for several values of the bias, including a fit to the data of the form $a_1 \tanh[(r-a_2)/a_3]+a_4 r^2+a_5$. Figure 5(b) shows the profile of the shearing rate, i.e., $\gamma=\partial v_\theta/\partial r$, derived from the fit. This technique is used to reduce the noise introduced by taking radial derivatives of the raw data. Below the transition threshold (75 V) the flow and flow shear is concentrated in the far edge plasma, and has not penetrated in to the cathode edge at $r \sim 28$ cm. As the threshold is reached (100 V), the peak value of the flow shear has not increased beyond the below-threshold value, but the flow has moved radially inward so that some finite flow shear exists near the cathode (plasma source) edge. As the bias is further increased, the flow amplitude and shear increase, but the shape of the profile is relatively unchanged. The observed transition is therefore not due to systematic increase of the shearing rate through a threshold value, but is instead associated with a sudden appearance of a large shearing rate at the plasma source edge.

If the change in radial transport rates is associated with shear suppression of turbulent transport, the shearing rate should be large enough to compete with characteristic timescales of the turbulence, often taken to be the linear growth rate or the nonlinear eddy turnover time. The turbulence in the edge of LAPD is known to be drift-Alfvén in nature,[27] and the characteristic frequency of drift waves is the diamagnetic drift frequency, i.e., $\omega_D=k_y v_{\mathrm{th,e}}\rho_e/L_n$ (where $k_y$ is the azimuthal wavenumber, $v_{\mathrm{th},e}$ is the electron thermal speed and $\rho_e$ is the electron gyroradius). The drift frequency will be taken as a proxy for the linear growth rate, although the growth rate of resistively driven modes is often only a small fraction of this frequency.[28] The nonlinear timescale in the turbulence, the eddy turnover time, can be estimated from measurements of the autocorrelation time in the turbulence, $\tau_{\mathrm{ac}}$. Figure 6 shows the radial profile of shearing rate, $\tau_{\mathrm{ac}}^{-1}$ and $\omega_D$ for three bias values: 75 V (below threshold), 100 V (near threshold), and 175 V (above threshold). In the calculation of $\omega_D$, the effective azimuthal wave number of the fluctuations ($k_y$) is taken from spatial correlation measurements (detailed later in this paper) which show a dominant azimuthal mode number of $m \sim 10$. The autocorrelation time is derived from the lab-frame autocorrelation function computed from ion saturation current data, which is fit to the function $a_0 \cos(a_1\tau)\exp(-a_2|\tau|)$, where $\tau_{\mathrm{ac}}=1/a_2$. At the threshold for transition, the shearing rate in the edge region is comparable to the local diamagnetic drift frequency and the autocorrelation frequency ($1/\tau_{\mathrm{ac}}$). In a flowing plasma, the autocorrelation time in the lab frame is affected both by flow of turbulent structures past the probe as well as temporal decorrelation of turbulent structures in the plasma frame (the eddy lifetime).[29] The autocorrelation time due to flow of structures past the probe can be estimated as $\tau_v \sim w_\perp/v_{\mathrm{flow}}$, where $w_\perp$ is the azimuthal scale size of the turbulence (azimuthal correlation length) and $v_{\mathrm{flow}}$ is the azimuthal flow velocity. An estimate of $\tau_v^{-1}$ is shown for a bias of 175 V in Fig. 6(c), using an azimuthal scale size of $w_\perp \sim 10$ cm (mo-

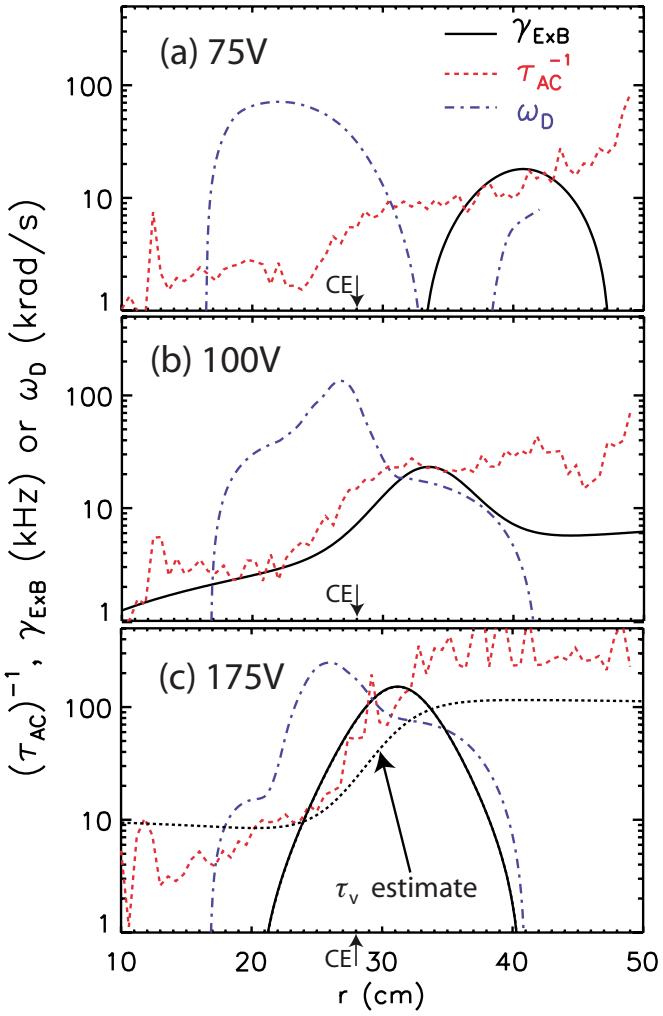


FIG. 6. (Color online) Radial profiles of the shearing rate ($\gamma_{E\times B}$), the turbulent inverse autocorrelation time ($\tau_{ac}^{-1}$), and the drift frequency ($\omega_D$) for three bias values: 75 V (below threshold), 100 V (near threshold), and 175 V (above threshold).

tivated by spatial correlation measurements). The $\tau_v^{-1}$ estimate is comparable to the calculated $\tau_{ac}^{-1}$, indicating that flow of structures past the probe is a major contributor to establishing the lab-frame autocorrelation time, and that it cannot be interpreted as a measure of the eddy turnover time. However, $\tau_{ac}$ does set a lower limit for the eddy turnover time and the actual plasma-frame eddy lifetime must be longer than $\tau_{ac}$ (and therefore $\tau_{eddy}^{-1}$ must be smaller than $\tau_{ac}^{-1}$). It is therefore reasonable to argue that the flow shear is large enough to be dynamically important and thus could suppress turbulent transport, leading to the observed confinement transition.

### B. Changes to spectrum and transport flux under biasing

Detailed measurements of turbulent spectra and turbulent particle flux have been performed to evaluate changes associated with the confinement transition. Figure 7 shows the radial profile of rms $I_{sat}$ fluctuations, contours of the $I_{sat}$ power spectrum, and the profile of perpendicular Mach number for several values of the rotation bias. All are time-averaged over the length of the bias pulse. The normalized fluctuation amplitude is $\delta I_{sat}/I_{sat} \sim 33\%$ at the peak of the fluctuation amplitude in the unbiased case. The fluctuation spectrum is broadband prior to biasing, with no evidence for coherent modes. Below threshold (75 V), some reduction of fluctuation amplitude is seen in the far edge, as well as a Doppler upshift in the fluctuation spectrum (especially associated with the strong flow feature near the wall at $r=50$ cm). As the transition threshold is approached (100 V) and exceeded (150 V), the fluctuation amplitude is reduced and concentrates on the steepened density gradient, but the spectrum remains broadband. The rearrangement of the fluctuation profile accompanies changes in the plasma density profile (not shown). A strong Doppler shift is also observed in the spectrum localized to the region of strong azimuthal flow.

Radial decorrelation, or reduction of the radial size of turbulent eddies, is one possible mechanism by which turbulent transport might be suppressed by sheared flow. Measurements of the two-dimensional (cross-field) turbulent correlation function have been performed to evaluate the role of this mechanism in the confinement transition. Figure 8 shows measurements of the two-dimensional correlation function of fluctuations in ion saturation current for unbiased and strongly biased (220 V) cases. These measurements are made using two probes separated along the magnetic field by 0.69 m. One probe is fixed in space near the cathode edge (at $r=26$ cm) and used as a reference to correlate against, while the second probe is moved shot-to-shot to make measurements at 775 locations in the plane perpendicular to the background magnetic field (the density gradient is in the $-\hat{x}$ direction). Prior to biasing, the correlation function is nearly isotropic, with a slightly longer correlation length in the radial direction ($\hat{x}$ in the figure). The correlation lengths in the unbiased case (radial and azimuthal) are $\lesssim 5$ cm, around five times the ion sound gyroradius and ten times the ion gyroradius. Under biasing, the azimuthal ($\hat{y}$) correlation length increases dramatically. However, the radial extent of the correlation function is not reduced significantly and therefore no strong evidence for radial decorrelation is found. In addition, a clear pattern of maxima and minima are visible in the correlation pattern measured in the rotating plasma. This pattern resembles the pattern expected of a coherent, high-$m$-number cylindrical eigenmode.

There are two potential explanations for transport reduction based on the measured correlation function. First, because the correlation function is strongly elongated in the presence of the flow, the eddy turnover time is lengthened: it takes longer for a blob of plasma to travel from one side of the eddy to the other in the radial direction. Thus, the effective transport time step is lengthened (i.e., the eddy turnover time increases), even though the step size (the radial correlation length) is largely unchanged. This explanation seems inconsistent with Fig. 6, which shows the autocorrelation time decreasing with increasing bias. However, the lab-frame autocorrelation time may be dominated by flow effects. Second, the spatial coherency of the fluctuations has increased dramatically as a result of the biasing. Turbulent particle diffusion is effective only in the presence of decorrelation: co-

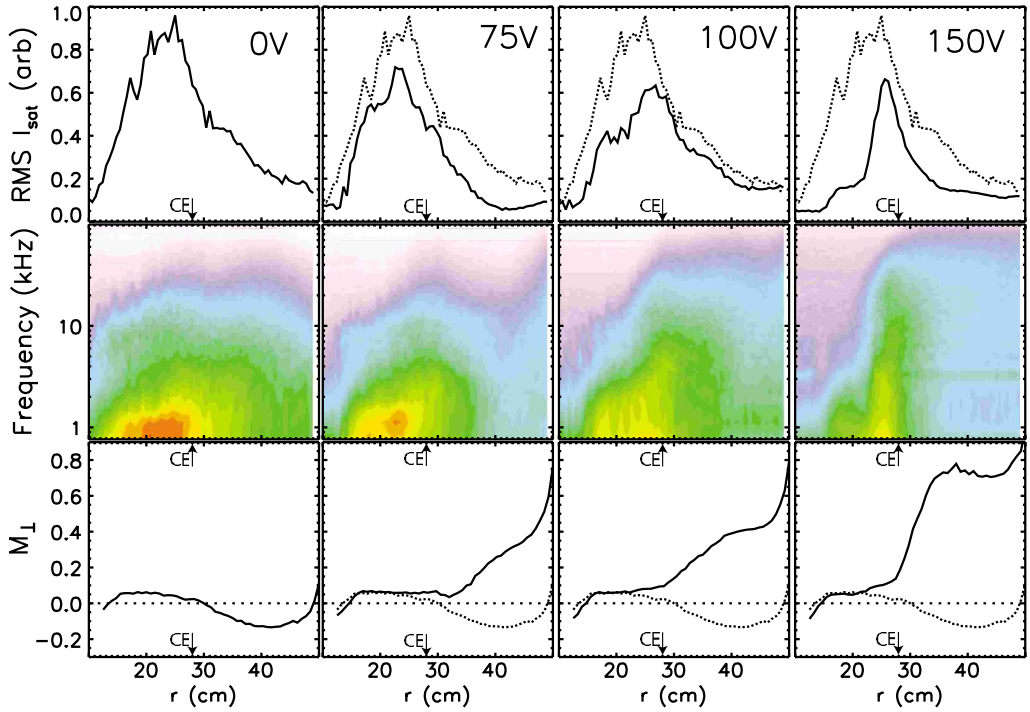


FIG. 7. (Color online) Radial profile of rms $I_{sat}$ fluctuations, Contours of $I_{sat}$ power spectrum vs radius and frequency, and Mach number profile for several bias values. The radial profiles of rms fluctuation level and Mach number in the unbiased case are shown as dashed lines for comparison with the biased cases.

herent vortices can flatten the density profile over their width through mixing, but do not lead to radial diffusion.

The expression for particle flux given in Eq. (1) can be directly evaluated using data obtained by a particle flux probe. Ion saturation current is measured to determine density fluctuations while floating potential is measured at two azimuthally separated probe tips in order to estimate fluctuations in the azimuthal electric field $E_\theta$. Figure 9(a) shows the radial profile of turbulent particle flux measured for four different bias voltages. The flux is computed using the fast Fourier transform (FFT) of the ion saturation current and electric field fluctuations, taking the final 2.6 ms of the 4 ms bias pulse as the window for the FFT computation. The measured particle flux is reduced and then suppressed as the bias is increased to 110 V (just past the threshold voltage). As the bias is further increased, there is a reversal in the measured particle flux indicating inward transport. The particle flux in Eq. (1) is established by the fluctuation amplitudes and the cross-coherency and cross-phase between density and electric field fluctuations. Figures 9(b) and 9(c) show the radial profiles of density and electric field fluctuations for the same bias voltages. The density fluctuations become more localized in space (peaked on the steepened density gradient), but the peak amplitude does not decrease significantly. The electric field fluctuations in the gradient region are also slightly reduced after the threshold is exceeded. However, electric field fluctuations grow stronger in the far edge with increased bias. As noted earlier, measurements of electric field fluctuations (and hence computed particle flux) are suspect in the presence of primary electrons ($r \lesssim 28$ cm). The radial region in which primary electrons are present is specifically marked in Figs. 9(a) and 9(c).

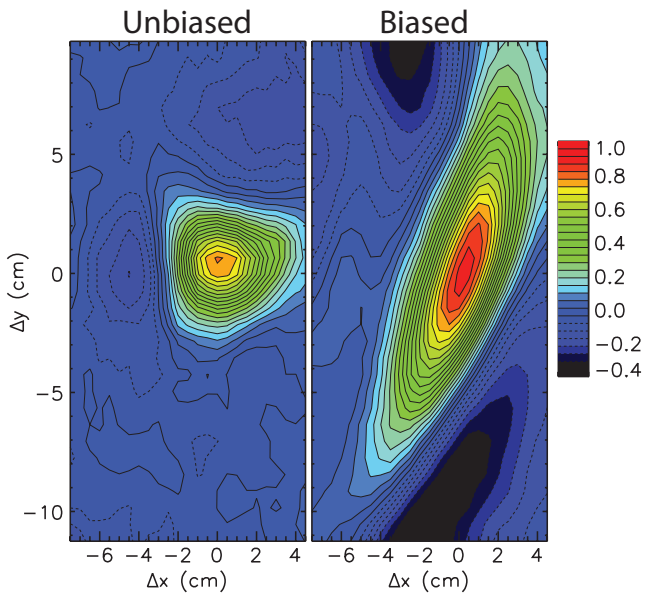


FIG. 8. (Color) Two-dimensional cross-field correlation function for $I_{sat}$ fluctuations in unbiased and biased plasmas.

The fast Fourier transform power spectrum of $I_{sat}$ fluctuations is shown in Fig. 10(a) (averaged over spatial locations 28 cm $< r <$ 30 cm). The spectrum is broadband before and after the transition, with decreased power at low frequency and a Doppler upshift in the spectrum apparent with increasing rotation. The cross-coherency between density and electric field fluctuations actually increases with bias, as shown in Fig. 10(c). Although the electric field fluctuation amplitude does decrease, the dominant cause of the observed flux behavior with bias appears to be changes in the cross-

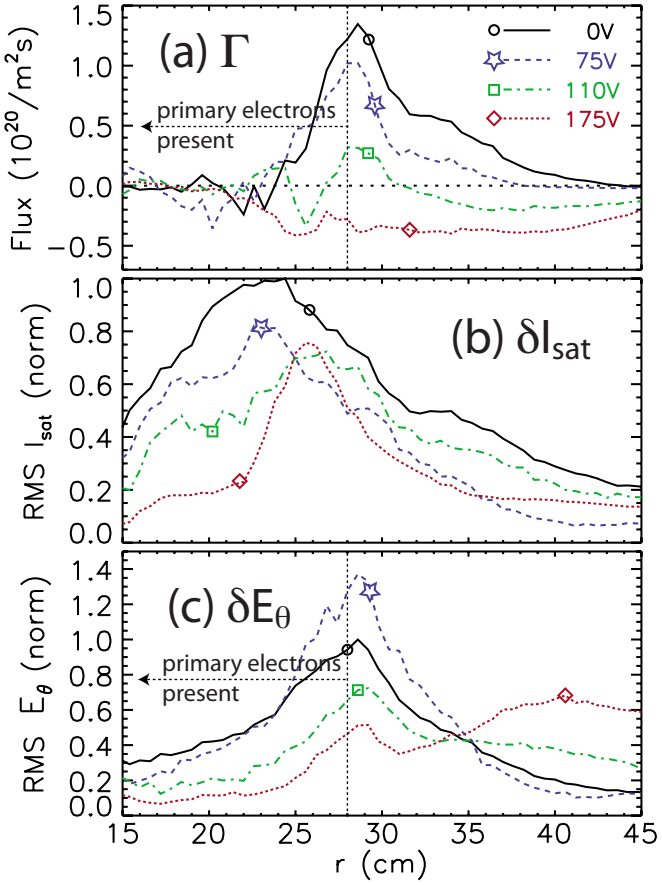


FIG. 9. (Color online) (a) Particle flux profile, (b) rms $I_{sat}$ fluctuation profile, and (c) rms $E_\theta$ fluctuation profile for several bias values.

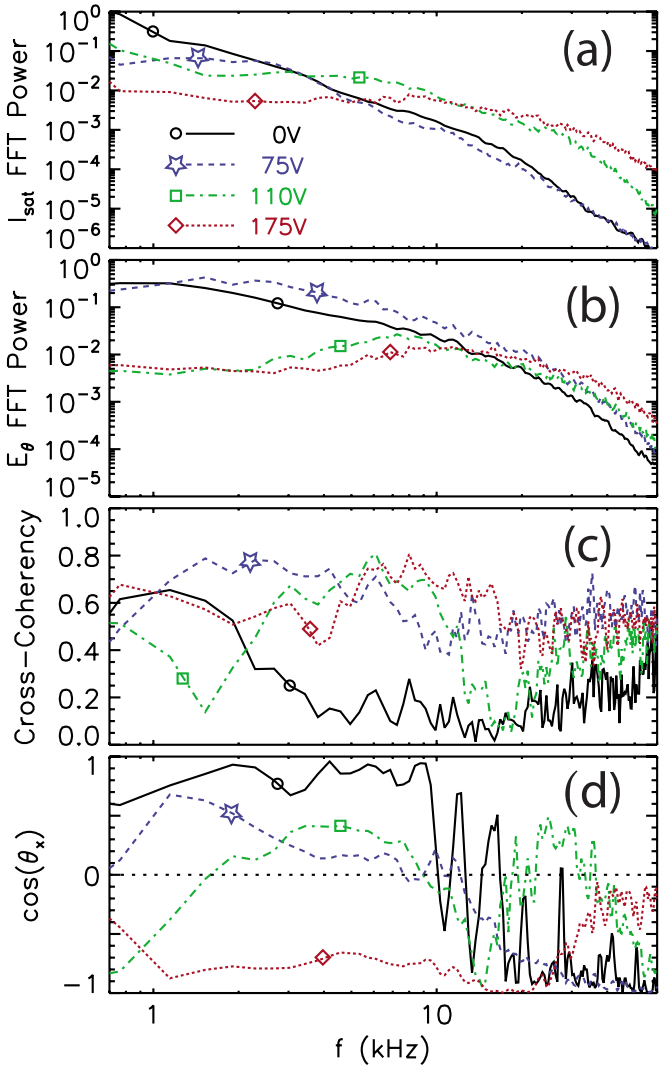


FIG. 10. (Color online) For the same bias values, averaged over $28<r<30$ cm and using a 2.6 ms time window at the end of the bias pulse for the FFT: (a) $I_{sat}$ FFT power spectrum, (b) $E_\theta$ FFT power spectrum, (c) cross-coherency, and (d) cross-phase between $I_{sat}$ and $E_\theta$.

phase. As shown in Fig. 10(d), the cosine of the cross-phase is very favorable for outward transport below the threshold, is modified to near zero around the threshold, and finally reverses sign at larger bias values.

Figure 11 shows a comparison between the radial profiles of the measured flux and the flux determined from transport analysis.[18] In the unbiased, nonrotating case, the measured and predicted flux agree remarkably well on field lines that do not connect to the cathode ($r>28$ cm). However, on cathode connected field lines (where primary electrons exist), the measured flux is near zero. One possible explanation for these observations is the influence of 50 eV primary electrons from the source on the floating potential measurement. The fastest electrons establish floating potential, and on the cathode-connected field lines, these are the primary electrons and not the bulk electrons ($T_e \sim 5$ eV). The primaries may not participate in the drift-wave dynamics or if they do, they have extremely long mean free path (comparable to the machine size) and any perturbation imparted on them might be phase-mixed away as they are highly nonlocal in the wave. Figure 9 is consistent with this argument, showing that the electric field fluctuations peak outside of the cathode radius while fluctuations in $I_{sat}$ (which is measured with $V_{bias} \sim 70$ V to reject primary electrons) peak further inward.

Inward flux (up the density gradient) is measured in these experiments at larger values of wall bias, while the transport model flux of the rotating plasma is nearly zero (classical transport). Inward flux has been reported in other biasing experiments on toroidal confinement devices[12,30] and also in the presence of turbulently driven large-scale shear flows in a cylindrical device.[31] In addition, turbulence-driven particle pinches are predicted theoretically in the presence of strongly sheared flow.[32] However, if the turbulence is driven purely by density gradients, only local reversal of the flux is allowed, not reversal across the whole profile, as observed here (thermodynamically, the density gradient can not steepen itself). The growth of electric field fluctuations in the far edge (away from density gradients; see Fig. 9) at large bias may be due to a new instability driven by other free energy sources such as the flow. It is possible that these new fluctuations could drive the observed inward flux. However, the measured inward flux cannot be consistent with transport modeling unless a source of plasma is present in the far edge region ($r>28$ cm) to feed the measured large inward flux. No primary electrons are present in this region, but ionization associated with rotation-heated bulk electrons might

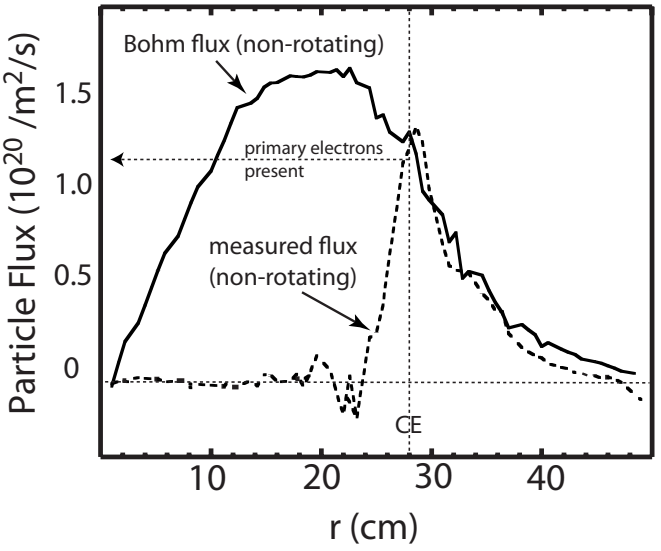


FIG. 11. Comparison between model and measured fluxes. Primary electrons may influence the ability to measure transport flux, and the region where they exist is marked in the figure.

provide an ionization source. The source of the apparent flux reversal in these measurements will be the subject of future work.

### C. Dynamics of the confinement transition

The temporal behavior of the azimuthal flow, turbulence, and flow profile shape during the confinement transition is interesting and provides further support for the conclusion that the radial flow profile is central to the transport reduction. In this section we focus on the relation of the shear rate profile to the density gradient profile. Figure 12 presents contour plots of density gradient, rms fluctuation amplitude ($I_{sat}$ fluctuations), and shearing rate versus radius and time for a case where a confinement transition occurs (125 V bias). The 125 V bias is applied from $t=7.5$ ms to $t=11.5$ ms (both marked with dotted lines in the figure). After the bias is turned on, the flow shear penetrates into the cathode edge,

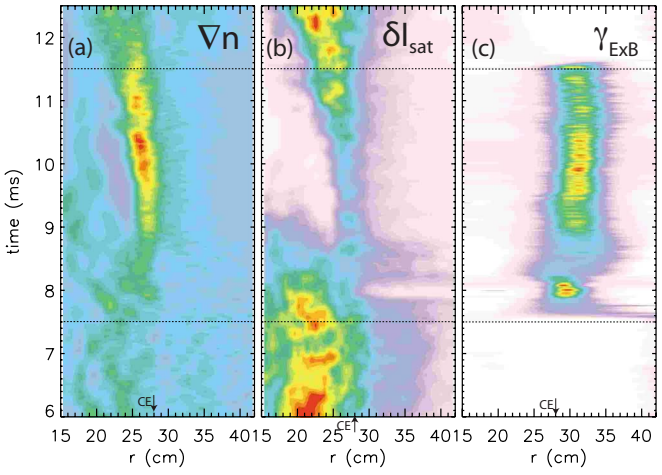


FIG. 12. (Color online) Contour plots of density gradient, rms $I_{sat}$ fluctuation amplitude, and shearing rate vs radius and time for 125 V bias.

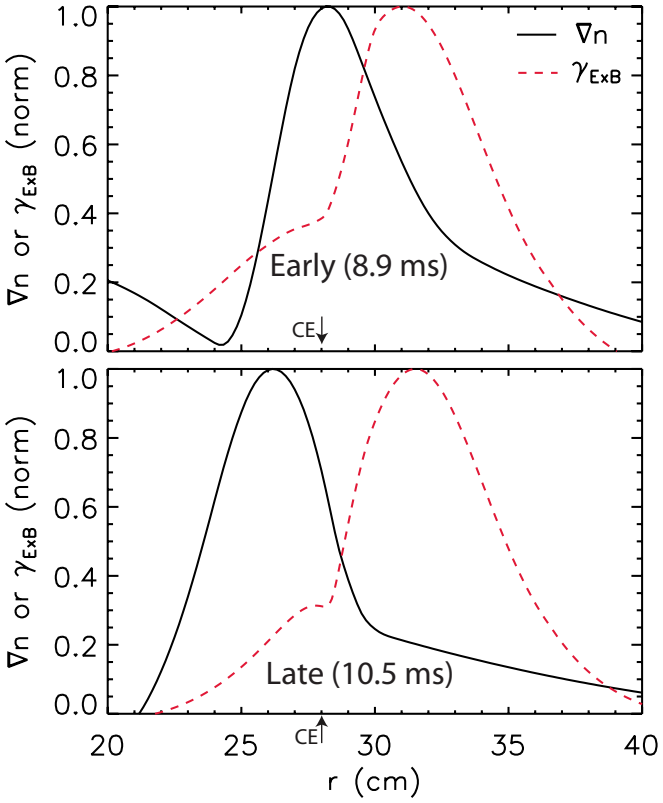


FIG. 13. (Color online) (Profiles of density gradient and shearing rate, derived from fits to the density and flow, early and late in the bias pulse.

where it peaks strongly at $t\approx 8$ ms. The first effect of the flow penetration is an immediate reduction in the fluctuation amplitude in the edge region ($30<r<35$). The negative correlation between flow shear and edge fluctuation amplitude is especially apparent near the first strong peak in the shear ($t\approx 8$ ms). The fluctuations further into the core plasma are suppressed more slowly, but reach their lowest levels 1.5 ms after the bias is turned on. On a similar timescale, the steepening of the edge density profile occurs and the core profile flattens. It is therefore likely that the reduction of core fluctuations is at least in part due to changes in the linear drive of the drift-Alfvén waves due to core density profile flattening. The steepening of the edge density gradient occurs on a timescale consistent with the transport timescale set by end losses along the straight magnetic field.[18]

After the initial transient, the density profile steepens and the shearing rate settles into a profile which persists in a quasi-steady state (from $t\approx 9$ ms to $t\approx 10.5$ ms). The fluctuation amplitude is reduced from the pretransition value, and is localized to the edge gradient region. However, late in the bias pulse (near $t\sim 10.5$ ms) the fluctuation amplitude increases again and the density gradient reduces. This observation can be explained by considering the overlap of the shear and density gradient profiles. From Fig. 12(b) and 12(c) it is apparent that late in the bias pulse the location of peak shear is slowly moving radially outward while the location of peak density gradient is moving radially inward. This is made clearer in Fig. 13, which shows the radial profile of density gradient and shearing rate, derived from fits, at two points in time. To emphasize profile shape and overlap,

the profiles are normalized to their peak values. Early in the quasi-steady phase (t=8.9 ms), significant overlap is seen between the density gradient and shearing rate profiles. However, later in the bias pulse ($t$=10.5 ms) the two profiles have moved apart and the amount of overlap is reduced substantially. Because of the reduced overlap between the density gradient (where linear drive for the turbulence exists) and the shearing rate, shear suppression of the turbulence should be less effective. This reduced suppression ability can explain the return of fluctuations and turbulent transport with the resultant reduction in the density gradient. Note that, since similar arguments could be made for the overlap of the density and flow profiles (these are the radial integrals of the profiles shown), it is not clear which profiles are determinant. However, it certainly appears that the degree of overlap between the profiles, whether density gradient and shear rate or density and flow, is crucial to the stabilization process.

## IV. CONCLUSIONS

Biasing the central chamber wall of the LAPD, positive with respect to the cathode, produces a rotation layer on field lines external to the cathode. This rotation layer leads to a significant reduction in radial transport of plasma. The reduction is accompanied by changes in the radial temperature and density profiles of the plasma column. In particular the density gradient scale length is greatly reduced near the source edge due to the reduction in radial transport rates. For a fixed bias pulse length, a threshold for reduction in radial transport exists. The threshold voltage is apparently determined by radial penetration of the flow into the gradient region of the plasma. Once the flow penetrates, a large flow and flow shear are immediately present in the gradient region and therefore a threshold value for the shearing rate cannot be determined from this experiment.

Without rotation, ion saturation current fluctuations are broadly distributed from the core to the plasma wall with peak amplitude very near, but inside, the cathode edge. As plasma rotation proceeds, the fluctuation profile adjusts with the changing density profile of the plasma. The fluctuations become concentrated in the gradient region of the plasma and the peak amplitude is reduced by a few tens of percent from the nonrotating value. The most dramatic change in the ion saturation fluctuations is noticed in the cross-field correlation function. In the nonrotating plasma, the cross-field correlation function is very nearly isotropic. In the rotating plasma, the radial correlation length is about the same as in the nonrotating plasma. However, the azimuthal correlation length of the rotating plasma is much longer than the radial correlation length (by about a factor of 5), and the correlation function takes on a noticeable structure, as might be expected for a coherent cylindrical eigenfunction.

The most significant change in the cross-correlation between azimuthal electric field fluctuations (floating potential) and density fluctuations (ion saturation current) occurs in the cross-phase in the frequency range below 10 kHz (about a tenth of the ion gyrofrequency). The cross-phase changes systematically with increasing rotation bias. In the unbiased, nonrotating plasma the cross-phase is near unity at low frequencies. As the rotation bias increases the cross-phase decreases toward zero and then progresses towards minus one for the fully rotating plasma. The measured radial fluxes calculated from the cross-correlation given in Eq. (1) agree with previous modeling results for the nonrotating plasma on field lines outside the cathode; i.e., in the absence of fast tails. In the rotating plasma the cross-correlation technique predicts negative (inward) fluxes that are inconsistent with modeling.

The change in radial transport depends upon the degree of spatial overlap between the shear rate and density gradient profiles as demonstrated by the behavior near threshold. The recovery of radial transport and subsequent increase in the scale length of the density profile, as observed late in the 125 V bias case, is accompanied by a decrease in the overlap between these two profiles. Thus, the stabilization process depends upon the spatial distribution of the azimuthal flow.

In these experiments, azimuthal flow was driven externally, and the interaction between the driven flow and spontaneously driven turbulence was studied. A critically important, unresolved issue in confinement transitions (e.g., L- to H-mode transition) is the mechanism behind the spontaneous generation of radial electric field and associated sheared flows. Many mechanisms have been proposed, including nonambipolar edge transport, neoclassical effects, and turbulent processes.[4,33–37] In particular, the self-generation of flows by turbulence (e.g., zonal flows) has received a great deal of attention as a likely candidate to explain spontaneous confinement transitions.[4,37] Direct evidence for Reynolds-stress-driven flow has been reported in a cylindrical device[38] and evidence for enhanced mode-coupling prior to the L- to H-transition has been seen in DIII-D[36,39] (however, similar, but not exhaustive, measurements in NSTX did not reveal enhanced mode-coupling[40]). Spontaneous azimuthal flows are observed in LAPD prior to biasing [see Fig. 2(b)] and future work will explore the role of inverse cascade and mode-mode coupling on generation of flows and flow-turbulence interaction in LAPD. Future work will also consider the role of sheath-driven processes present in open-magnetic-field-line configurations in flow generation.[41]

## ACKNOWLEDGMENTS

The authors would like to acknowledge the contributions of R. J. Taylor and P. Pribyl in establishing the ability to induce bias-driven rotation in LAPD. These experiments were performed using the Basic Plasma Science Facility at UCLA, which is supported by DOE and NSF. T.A.C. acknowledges support from DOE Fusion Science Center Cooperative Agreement DE-FC02-04ER54785 and NSF Grant No. PHY-0547572.

[1] P. C. Liewer, Nucl. Fusion **25**, 543 (1985).
[2] F. Wagner, G. Becker, K. Behringer, D. Campbell, A. Eberhagen, W. Engelhardt, G. Fussmann, O. Gehre, J. Gernhardt, G. Vongierke, G. Haas, M. Huang, F. Karger, M. Keilhacker, O. Kluber, M. Kornherr, K. Lackner, G. Lisitano, G. G. Lister, H. M. Mayer, D. Meisel, E. R. Muller, H. Murmann, H. Niedermeyer, W. Poschenrieder, H. Rapp, H. Rohr, F. Schneider, G. Siller, E. Speth, A. Stabler, K. H. Steuer, G. Venus, O. Vollmer, and Z. Yu, Phys. Rev. Lett. **49**, 1408 (1982).
[3] K. H. Burrell, Phys. Plasmas **4**, 1499 (1997).
[4] P. W. Terry, Rev. Mod. Phys. **72**, 109 (2000).

[5]R. J. Taylor, M. L. Brown, B. D. Fried, H. Grote, J. R. Liberati, G. J. Morales, P. Pribyl, D. Darrow, and M. Ono, Phys. Rev. Lett. **63**, 2365 (1989).
[6]G. R. Tynan, J. Liberati, P. Pribyl, R. J. Taylor, and B. Wells, Plasma Phys. Controlled Fusion **38**, 1301 (1996).
[7]R. R. Weynants, G. Van Oost, G. Bertschinger, J. Boedo, P. Brys, T. Delvigne, K. H. Dippel, F. Durodie, H. Euringer, K. H. Finken, D. S. Gray, J. D. Hey, D. L. Hillis, J. T. Hogan, L. Konen, R. Leners, A. M. Messian, A. Pospieszczyck, U. Samm, R. P. Schorn, B. Schweer, G. Telesca, R. Vannieuwenhove, and P. E. Vandenplas, Nucl. Fusion **32**, 837 (1992).
[8]J. Boedo, D. Gray, S. Jachmich, R. Conn, G. P. Terry, G. Tynan, G. Van Oost, R. R. Weynants, and T. Team, Nucl. Fusion **40**, 1397 (2000).
[9]C. Silva, H. Figueiredo, I. Nedzelskiy, B. Goncalves, and C. A. F. Varandas, Plasma Phys. Controlled Fusion **48**, 727 (2006).
[10]D. Craig, A. F. Almagri, J. K. Anderson, J. T. Chapman, C. S. Chiang, N. A. Crocker, D. J. DenHartog, G. Fiksel, S. C. Prager, J. S. Sarff, and M. R. Stoneking, Phys. Rev. Lett. **79**, 1865 (1997).
[11]B. E. Chapman, A. F. Almagri, J. K. Anderson, C. S. Chiang, D. Craig, G. Fiksel, N. E. Lanier, S. C. Prager, J. S. Sarff, M. R. Stoneking, and P. W. Terry, Phys. Plasmas **5**, 1848 (1998).
[12]M. G. Shats, K. Toi, K. Ohkuni, Y. Yoshimura, M. Osakabe, G. Matsunaga, M. Isobe, S. Nishimura, S. Okamura, K. Matsuoka, and C. Grp, Phys. Rev. Lett. **84**, 6042 (2000).
[13]O. Sakai, Y. Yasaka, and R. Itatani, Phys. Rev. Lett. **70**, 4071 (1993).
[14]H. Biglari, P. H. Diamond, and P. W. Terry, Phys. Fluids B **2**, 1 (1990).
[15]E. J. Powers, Nucl. Fusion **14**, 749 (1974).
[16]A. S. Ware, P. W. Terry, P. H. Diamond, and B. A. Carreras, Plasma Phys. Controlled Fusion **38**, 1343 (1996).
[17]R. A. Moyer, K. H. Burrell, T. N. Carlstrom, S. Coda, R. W. Conn, E. J. Doyle, P. Gohil, R. J. Groebner, J. Kim, R. Lehmer, W. A. Peebles, M. Porkolab, C. L. Rettig, T. L. Rhodes, R. P. Seraydarian, R. Stockdale, D. M. Thomas, G. R. Tynan, and J. G. Watkins, Phys. Plasmas **2**, 2397 (1995).
[18]J. E. Maggs, T. A. Carter, and R. J. Taylor, Phys. Plasmas **14**, 052507 (2007).
[19]W. Horton, J. C. Perez, T. Carter, and R. Bengtson, Phys. Plasmas **12**, 022303 (2005).
[20]J. C. Perez, W. Horton, R. D. Bengtson, and T. Carter, Phys. Plasmas **13**, 055701 (2006).
[21]W. Gekelman, H. Pfister, Z. Lucky, J. Bamber, D. Leneman, and J. Maggs, Rev. Sci. Instrum. **62**, 2875 (1991).
[22]D. Leneman, W. Gekelman, and J. Maggs, Rev. Sci. Instrum. **77**, 015108 (2006).
[23]P. Pribyl and W. Gekelman, Rev. Sci. Instrum. **75**, 669 (2004).
[24]S.-L. Chen and T. Sekiguchi, J. Appl. Phys. **36**, 2363 (1965).
[25]J. P. Gunn, C. Boucher, P. Devynck, I. Duran, K. Dyabilin, J. Horacek, M. Hron, J. Stockel, G. Van Oost, H. Van Goubergen, and F. Zacek, Phys. Plasmas **8**, 1995 (2001).
[26]T. Shikama, S. Kado, A. Okamoto, S. Kajita, and S. Tanaka, Phys. Plasmas **12**, 044504 (2005).
[27]J. E. Maggs and G. J. Morales, Phys. Plasmas **10**, 2267 (2003).
[28]W. Horton, Rev. Mod. Phys. **71**, 735 (1999).
[29]A. Bencze and S. Zoletnik, Phys. Plasmas **12**, 052323 (2005).
[30]J. A. Boedo, D. S. Gray, P. W. Terry, S. Jachmich, G. R. Tynan, R. W. Conn, and TEXTOR-94 Team, Nucl. Fusion **42**, 117 (2002).
[31]G. R. Tynan, C. Holland, J. H. Yu, A. James, D. Nishijima, M. Shimada, and N. Taheri, Plasma Phys. Controlled Fusion **48**, S51 (2006).
[32]P. W. Terry, D. E. Newman, and A. S. Ware, Phys. Plasmas **10**, 1066 (2003).
[33]S.-I. Itoh and K. Itoh, Phys. Rev. Lett. **60**, 2276 (1988).
[34]K. Itoh and S.-I. Itoh, Plasma Phys. Controlled Fusion **38**, 1 (1996).
[35]J. W. Connor and H. R. Wilson, Plasma Phys. Controlled Fusion **42**, R1 (2000).
[36]G. R. Tynan, R. A. Moyer, and M. J. Burin, Phys. Plasmas **8**, 2691 (2001).
[37]P. H. Diamond, S.-I. Itoh, K. Itoh, and T. A. Hahm, Plasma Phys. Controlled Fusion **47**, R35 (2005).
[38]C. Holland, J. H. Yu, A. James, D. Nishikima, M. Shimada, N. Taheri, and G. R. Tynan, Phys. Rev. Lett. **96**, 195002 (2006).
[39]R. A. Moyer, G. R. Tynan, C. Holland, and M. J. Burin, Phys. Rev. Lett. **87**, 135001 (2001).
[40]A. E. White, S. J. Zweben, M. J. Burin, T. A. Carter, T. S. Hahm, J. A. Krommes, and R. J. Maqueda, Phys. Plasmas **13**, 072301 (2006).
[41]P. Ricci, B. N. Rogers, and S. Brunner, Phys. Rev. Lett. **100**, 225002 (2008).